Coaxial poly(lactic acid) electrospun composite membranes incorporating cellulose and chitin nanocrystals

Please, cite as follows:

Blanca Jalvo, Aji P. Mathew, Roberto Rosal, Coaxial poly(lactic acid) electrospun composite membranes incorporating cellulose and chitin nanocrystals, In Journal of Membrane Science, Volume 544, 2017, Pages 261-271, ISSN 0376-7388, https://doi.org/10.1016/j.memsci.2017.09.033.

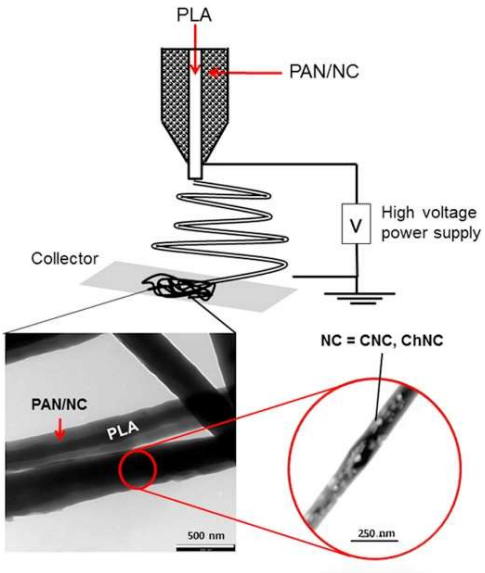

http://www.sciencedirect.com/science/article/pii/S0376738817320549

Coaxial poly(lactic acid) electrospun composite membranes incorporating cellulose and chitin nanocrystals

Blanca Jalvo[1], Aji P. Mathew[2,*], Roberto Rosal[1,*]

[1] Department of Chemical Engineering, University of Alcalá, E-28871 Alcalá de Henares, Madrid, Spain
[2] Department of Materials and Environmental Chemistry, Stockholm University, Stockholm, Sweden

* Corresponding authors: aji.mathew@mmk.su.se, roberto.rosal@uah.es

Abstract

In this study, we used electrospinning to produce core-shell nanofibers of poly(lactic acid) as core and polyacrylonitrile/cellulose nanocrystals (CNC) or polyacrylonitrile/chitin nanocrystals (ChNC) as shell. Electrospun materials prepared at different nanocrystal concentrations were tested and assayed as microfiltration membranes. The coaxial membranes presented a maximum pore size in the 1.2–2.6 μm range and rejections > 85% for bacterial cells (0.5 × 2.0 μm) and > 99% for fungal spores (> 2 μm). The morphological and mechanical properties and the water permeability of the nanocomposite membranes were studied. The morphological characterization showed random fibers of beadless and well-defined core/shell structured fibers with diameter generally below the micron size with presence of secondary ultrafine nanofibers. Tensile strength and Young's modulus of elasticity improved with respect to coaxial membranes without nanocrystals with best mechanical properties achieved at 5 wt% CNC and 15 wt% ChNC loadings. The enhancement was attributed to the reinforcing effect of the percolating network of cellulose nanocrystals. Water permeability increased for all membranes loaded with nanocrystals with respect to the coaxial fibers without nanocrystals, the highest corresponding to ChNC composites with up to a 240% increase over non-loaded membranes. Composite membranes prepared with CNC in their shell were hydrophilic, in contrast with the hydrophobic PLA core, while coaxial fibers with ChNC were superhydrophilic. CNC membranes were negatively charged but ChNC originated neutral or positively charged membranes due to the contribution of deacetylated chitin structural units. Upon exposure to E. coli cultures, composite membranes containing ChNC showed a high antimicrobial action and were essentially free of bacterial colonization under strong biofilm formation conditions.

Keywords: Coaxial electrospinning; Poly(lactic acid); Cellulose nanocrystals; Chitin nanocrystals; Antimicrobial materials

1. Introduction

Electrospinning is a versatile procedure for producing polymeric fibers below the micron scale [1]. The technique has been recently investigated in view of its potential to generate high surface-to-volume ratio materials functionalized in the nanoscale [2,3]. By controlling operating conditions and solution parameters, electrospinning can be used to produce a variety of non-woven porous or smooth nanofibrous structures suitable for their use as filtration media [4]. Opposite to conventional membrane preparation technologies, such as phase inversion, the high pore interconnectivity and porosity of electrospun membranes make them promising materials for filtration processes [5]. However, filtration using electrospun fibrous membranes must overcome the hurdle of their lower mechanical strength compared to polymeric films, which is particularly critical in pressure-driven filtration for water treatment applications [6]. The reason is the low degree of molecular orientation in electrospun polymers, which is a consequence of the competition between flow-induced chain orientation and chain relaxation before fiber solidification [7]. The mechanical properties of electrospun fibers can be improved using post-treatments, such as stretching and annealing, that increase molecular orientation and crystallinity [8]. Alternatively, the co-electrospinning of polymers and fillers can produce composite fibers with enhanced mechanical properties [9,10].

Biofouling, is one of the main factors determining membrane performance in many practical applications [11]. It refers to the growth of microorganisms on membrane surface, and results in loss of permeability, increased transmembrane pressure, reduced membrane life and risk of pathogen dissemination [12]. Two approaches can be followed to minimize biofouling: Proper surface design to prevent primary adhesion, or the use of cleaning strategies including the use of biocides [13]. The manipulation of the physicochemical properties of membranes allow creating surfaces hostile for microbial attachment targeting the initial stage of microbial colonization, before biofilm formation [14]. Biofilms are complex communities of cells embedded in an extracellular polymeric matrix formed by polysaccharides, proteins, and nucleic acids, which protect cells from adverse conditions [15]. Once formed, biofilms are very difficult to remove. In fact, biofilm formation constitutes an advantageous strategy for survival and growth in hostile environments and represents a degree of complexity in structure and metabolism similar to the tissues of higher organisms

[16]. The high tunability of electrospun membranes offers new ways of creating antimicrobial environments. The incorporation of functional agents with antibiotic properties [17], the use of polymers with intrinsic antibacterial properties such as chitosan [18] and different treatments for surface modification [19] have been explored to create biofouling resistant electrospun fibers.

Poly(lactic acid), PLA, is a biodegradable thermoplastic aliphatic polyester derived from renewable resources, which, despite being hydrophobic, displays higher natural hydrophilicity than conventional hydrophobic thermoplastic polymers due to the better access of water molecules to the polar oxygen linkages of its backbone. Higher water fluxes and reduced biofouling tendency of PLA-based membranes offer a good option to replace conventional membranes made of petrochemical polymers [20]. However, electrospun PLA in membrane applications presents some limitations due to the poor mechanical properties of pure PLA fibers [5].

Cellulose and chitin fibrils in the nanometer range are biobased nanoparticles that expanded the possibilities of natural polymers in the field of engineered sustainable nanocomposites [21]. The dimensions of cellulose and chitin nanocrystals and nanofibers offer a high surface area filler and the possibility of creating functional materials with exceptional physical, chemical and mechanical properties [22]. Cellulose nanocrystals from microcrystalline cellulose were previously reported to substantially improve the mechanical properties of electrospun nanocomposites prepared from PLA [23], polyethylene oxide [24], and polyacrylamide [25].

Chitin, poly-β-(1-4)-N-acetyl-D-glucosamine, is a natural, renewable and biodegradable polymer, the second most abundant natural polymer after cellulose. Substantial amounts of this structural material can be found in animals, as part of exoskeletons, backbones and the cell walls of fungi and yeasts. Despite its easy accessibility, chitin is an underutilized resource because of its insolubility in water and common organic solvents [26]. However, in recent times the use of chitin has generated great interest due to its excellent mechanical and certain antibacterial properties. The incorporation of chitin derived nanocrystals to different polymeric membranes has been recently addressed with the purpose of enhancing their mechanical properties and antifouling performance [27,28].

In this work, structured electrospun PLA fibers reinforced with chitin and cellulose nanocrystals were prepared by means of coaxial electrospinning and used to prepare a microfiltration membrane with size exclusion in the low-micrometer range. Several works already reported the impact of nanocrystalline cellulose on the physical properties of PLA composites. It has been described that the resulting nanocomposites displayed a considerable improvement in mechanical properties, greater at temperatures below the glass transition temperature of PLA due to the enhancement of its crystallinity degree [29–32]. Our approach was to create core-shell fibers with nanocrystals on the fiber surface in order to deeply modify the physicochemical properties of membrane surface to enhance water permeability and resistance to microbial attachment. The described methodology aimed at combining the environmentally desirable properties of PLA with the unique characteristics of cellulose/chitin nanocrystals to create high flux and low biofouling membranes with enhanced mechanical resistance.

2. Experimental

2.1. Materials

Transparent PLA (marketed under trade name PLA Polymer 2002D) was acquired in pellets from NatureWorks LLC, UK, with melt index (MFR) of 5–7 g/10 min (at 210 °C/2.16 kg), molecular weight 121,400 g/mol, melting temperature 160 °C and 4% D-content (96% L-lactide). Polyacrylonitrile (PAN), molecular weight 150,000, melting temperature 317 °C, was obtained from Sigma-Aldrich. *N, N*-dimethylformamide (DMF, synthesis grade) and chloroform (synthesis grade) were purchased from Scharlab (Spain). Culture media components were biological grade reagents acquired from Conda-Pronadisa (Spain). Fluorescein diacetate (FDA), Live/Dead Bac-Light Bacterial Viability Kit and FilmTracer SYPRO Ruby were acquired from Invitrogen (Thermo Fisher, Waltham, USA).

The first type of cellulose nanocrystals, CNC_{H2SO4}, was prepared via sulfuric acid hydrolysis. Briefly, microcrystalline cellulose was mixed with sulfuric acid (63.5 wt%) under stirring in an ice bath. The suspension was heated up to 44 °C for 130 min under stirring. Then, the suspension was centrifuged for 10 min at 12,000 rpm until the supernatant became turbid. The nanocrystal suspension was neutralized against deionized water through dialysis. Thereafter, the suspension was sonicated in an ice bath to separate the nanocrystals [33].

The second kind of cellulose nanocrystals, CNC_{BE}, were obtained following the bioethanol processing route [34,35]. Unbarked wood was hydrolyzed using dilute acid in a bioethanol pilot plant at SP Processum, Örnsköldsvik, Sweden, and refined to obtain pure cellulose. The refining was done by Soxhlet extraction for 6 h at 150 °C using toluene/acetone mixture (2:1 ratio). This material was then bleached, washed with deionized water and concentrated by centrifugation to 17 wt%. The purified cellulose from bioethanol process was led to 2 wt% suspensions, mixed by shear mixture and passed through the homogenizer, 10 times to obtain a thick gel of cellulose nanocrystals (CNC_{BE}) as reported elsewhere [35].

Chitin nanocrystals (ChNC) were isolated from crab shells using hydrochloric acid hydrolysis. The raw material was boiled in 5 wt% KOH solution for 6 h

under stirring to remove proteins. Afterwards, the suspension was washed with distilled water and then bleached with chlorite at 80 °C for 6 h. Thereafter, the bleached suspension was washed followed by bleaching during overnight treatment using 5 wt% KOH and then concentrated using centrifuge. After that, the purified chitin was hydrolyzed using HCl 3 N for 90 min at 80 °C under stirring. After hydrolysis, the excess acid was removed by centrifugation until the turbid supernatant was achieved. The isolation process was completed by neutralization against deionized water. Then, the suspension was sonicated to individualize the nanocrystals [36,37]. In what follows, CNC_{H2SO4} and CNC_{BE} will be jointly referred to as cellulose nanocrystals, CNC, while the term nanocrystals, NC, will include also chitin nanocrystals, ChNC. Water dispersed NC were solvent exchanged into DMF by distillation-assisted evaporation to facilitate the electrospinning process.

2.2. Coaxial electrospinning

Fig. 1 presents a schematic illustration of the experimental setup used for coaxial electrospinning. The spinneret consisted of a double capillary tube in which the smaller was concentrically inserted into the larger one. The inner fluid produced the core of the fiber, while the outer one formed the shell of core-shell or coaxial fibers. 7 wt% PLA in chloroform/DMF (3:2 v/v) was used for the core and 10 wt% of PAN in DMF with 5, 10, 15 or 20 wt% of NC (in solvent-free basis) was used to produce the PAN/NC fiber shell. The choice of PAN as shell-forming polymer was based on its compatibility with NC, that did not agglomerate during electrospinning. Besides, the shell solution must be spinnable by itself and viscous enough guide the core one to attain coaxial architecture. Also, in the process of coaxial electrospinning, it is important to keep the viscosity ratio of shell and core solutions inside a certain value to produce uniform core–shell structures [38]. PAN met these constraints allowing the production of homogeneous coaxial fibers as described below. The shell mixture was sonicated using an ultrasonic probe VC505 (500 W, Sonics and Materials Inc.) for 5 min carried out in short intervals at 20% amplitude followed by 15 min of magnetic stirring at 80 °C. The flow rate of both solutions was maintained at a constant rate of 0.8 mL/h driven by a syringe pump (Harvard PHD 22/2000) and the voltage applied was 20 kV supplied by a high voltage power supply (Heinzinger LNC 30000). Electrospun nanofibers were deposited on a flat collector plate (16 cm × 16 cm) covered with aluminum foil and at 20 cm distance from the coaxial needle tip (Yflow SD, Spain). Each sample was collected for 6 h.

All the coaxial membranes prepared in this work have the same polymeric shell@core structure, PAN/NC@PLA. The changes in fiber composition are given by the type of nanocrystal and its concentration. The nomenclature used for the prepared membranes is shown in Table 1.

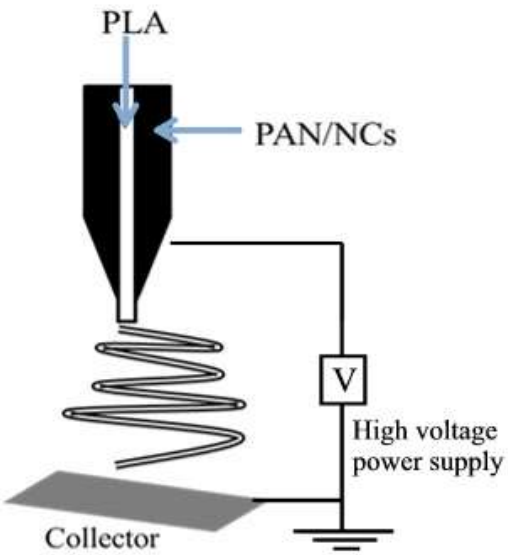

Figure 1. Schematic illustration of the coaxial electrospinning setup for core-shell fibers. Core: PLA; shell: PAN/NC.

2.3. Membrane characterization

The morphology of electrospun fibers was observed by scanning electron microscopy (SEM) using a Carl Zeiss DSM 950 instrument operating at 25 kV. The membranes were sputter coated with gold before SEM observations. Transmission electron microscopy (TEM) images of coaxial structures were obtained using a transmission electron microscope (Zeiss M10, Germany) at an accelerating voltage of 50 kV. AFM images were obtained using a Multimode Nanoscope V Atomic force microscope (AFM) from Bruker. Fiber diameters were calculated from the analysis of SEM images using ImageJ software from at least 50 nanofibers randomly selected from each image.

The wettability of membrane surfaces was tested using an optical contact angle meter (Krüss DSA25 Drop Shape Analysis System) using the sessile drop method. Samples were placed on the test cell and drops of distilled water were deposited on the surfaces by the delivering syringe. Contact angle measurements for each surface were taken at room temperature on at least three positions on each sample.

Surface zeta potential (ζ-potential) was measured via electrophoretic light scattering (Zetasizer Nano ZS) using the Surface Zeta Potential Cell (ZEN 1020) from Malvern. Measurements were performed at 25 °C using 10 mM KCl, aqueous solution pH 7.5, with of 0.5 wt% poly(acrylic acid) (450 kDa), for negatively charged membranes, and 0.5 wt% polyethylenimine (600 Da), for positively charged membranes, used as tracers. pH was adjusted using 1 M KOH or 1 M HCl.

2.4. Membrane permeability and microfiltration performance

A dead-end stainless steel filtration module (Filter Holder 47 mm, Millipore) with an effective membrane area of 11.3 cm^2 and equipped with nitrogen pressure

Table 1. Composition and nomenclature of electrospun membranes[a].

Fibre type	Membrane identifier	Shell nanocrystal	Nanocrystal wt% [b]
	PLA	-	-
PAN@PLA	PAN@PLA	-	-
PAN/NC@PLA	PAN/$CNC_{H_2SO_4}$-5@PLA	Cellulose H_2SO_4	5
	PAN/$CNC_{H_2SO_4}$-10@PLA	Cellulose H_2SO_4	10
	PAN/$CNC_{H_2SO_4}$-15@PLA	Cellulose H_2SO_4	15
	PAN/$CNC_{H_2SO_4}$-20@PLA	Cellulose H_2SO_4	20
	PAN/CNC_{BE}-5@PLA	Cellulose BE	5
	PAN/CNC_{BE}-10@PLA	Cellulose BE	10
	PAN/CNC_{BE}-15@PLA	Cellulose BE	15
	PAN/CNC_{BE}-20@PLA	Cellulose BE	20
	PAN/ChNC-5@PLA	Chitin	5
	PAN/ChNC-10@PLA	Chitin	10
	PAN/ChNC-15@PLA	Chitin	15
	PAN/ChNC-20@PLA	Chitin	20

[a] In all cases, PLA concentration was 7 wt% (core polymer) and PAN concentration was 10 wt% (shell polymer). Accordingly, the ratio PLA/PAN in the final fibres was 7/10 in weight.
[b] In solvent-free basis.

control was used to measure the pure water flux, pore size and microfiltration performance of the nanofibrous membranes. Water permeability was measured using a constant transmembrane pressure of 0.2 bar. To open any possibly closed pores before the water flux test, freshly prepared membranes were pre-wetted and compacted at 0.5 bars for 5 min. Then, water flux was evaluated, and membrane permeability was determined from the pure water flux per unit transmembrane pressure.

The bubble point test for evaluating membrane maximum pore size was performed following the F316 Test Method described in American Society for Testing and Materials Standard (ASTM). Membranes, preconditioned by immersion in distilled water, were placed in a filter holder connected to a source of regulated gas pressure flowing upwards. The pressure of gas at the onset of bubble formation was recorded as bubble point and used to calculate the diameter of the larger membrane pores as follows:

$$d = \frac{4\gamma \cos\theta}{P} \quad (1)$$

where P is the bubble-point pressure, γ the surface tension of the liquid, θ the liquid-solid contact angle when a gas bubble is penetrating through a pore of its same radius (therefore, $\theta = 0$), and d the maximum pore average diameter.

Size exclusion experiments were performed by filtering suspensions of bacterial cells and mold spores. For it, the bacterial strain used was *Escherichia coli* CECT 516 (equivalent to ATCC 8739). Cell cultures grew overnight in Nutrient Bacterial medium (NB: for 1 L solution in distilled water, beef extract 5 g, peptone 10 g, NaCl 5 g, pH was adjusted to 7.2) while shaking at 37 °C. Reactivation was tracked by measuring optical density at 600 nm. For spore removal assays, spores of the fungi *Aspergillus niger* (ATCC 6275) were used after being resuspended in a saline solution (NaCl 0.9% w/v) to avoid their growth and the formation of mycelia. The microfiltration capacity of the membranes was assessed by filtering liquid cultures of *E. coli* and *A. niger* spores (10^7–10^8 cells/mL) for 60 min through all membrane specimens. The retention of microorganisms due to size exclusion was assessed by tracking the optical density at 600 nm of the filtrate, which was measured every 15 min. The reduction in pathogen concentration was calculated compared to the optical density of the feed suspension. Scanning electron microscopy (SEM) images of the surface of materials were obtained using a Hitachi S-3000N microscope operating at 25 kV. For this, a process of cell fixation in glutaraldehyde 5% (v/v) in 0.2 M sodium cacodylate buffer pH 7.2 was carried out 1 h at room temperature. Samples were then rinsed in cacodylate buffer and dehydrated in an ascending ethanol series (25%, 50%, 70%, 90% and 100%) before critical point drying with CO_2 and subsequent observation with SEM.

2.5. Mechanical properties

Membrane tensile strength and elongation at break were measured using a universal testing machine, Shimadzu Autograph AG-X with a load cell 500 N. Before taking measurements, test samples were preconditioned at 45% relative humidity for one week. Their thickness was measured using a digital thickness gauge. Samples of 50 mm length, 5 mm width and approximately 150 μm thickness were placed on paper windows with a preload of 0.1 N according to prescriptions. The speed of the strain testing was 2 mm/min and the tensile gauge length was 20 mm. At least 5 specimens were tested for each material. Ultimate tensile stress, σ_{max}, was calculated by dividing the maximum load of force

at failure, F, by the initial cross-sectional area of the membrane specimen, A_o:

$$\sigma_{max} = \frac{F}{A_o} \quad (2)$$

Fracture strain, ε, was calculated as elongation at break based on the initial sample length, L_0, and the sample length at break point, L:

$$\varepsilon = \ln\left(\frac{L}{L_o}\right) \quad (3)$$

Young's modulus was calculated through a linear regression analysis of the initial linear portion of the stress-strain curves.

2.5. Bioassays

The same bacterial strain used for size exclusion assays was also used for antimicrobial and antibiofouling bioassays. Biofilm formation was assessed for PLA and PAN/NC@PLA composites after placing membrane specimens on polystyrene 24-well plates. Exponentially growing cultures of *E. coli* on NB were diluted to an OD_{600} of 0.0138 (10^8 cells/mL). 2 mL of diluted cultures were placed on the surface of the electrospun membranes, which were subsequently incubated for 18 h at 37 °C without stirring. After the biofilm assay, the liquid culture was removed and membranes were carefully washed with distilled water to remove planktonic cells. For the quantification of biofilms, fluorescein diacetate (FDA) was used, following the manufacturer's instructions. The fluorescence was measured in a fluorometer/luminometer Fluoroskan Ascent FL as follows. 200 µL of the fluorescent stain were extended over the entire surface. After 15 min of incubation at 25 °C, FDA was excited at 485 nm, and emission recorded at 538 nm.

The visualization of cells and biofilms was performed by confocal microscopy 18 h after inoculation using a Leica Microsystems Confocal SP5 fluorescence microscope (Leica Microsystems, Germany). Viable and non-viable bacteria were tracked using Live/Dead BacLight Bacterial Viability Kit. For membrane staining, the surface of each specimen was covered with 30 µL of stain (a 0.5:1 mixture of SYTO 9 and PI in DMSO). The incubation was performed in the dark for 15–30 min at room temperature. For matrix visualization, the biofilms were stained with 200 µL FilmTracer SYPRO Ruby per film, incubated in the dark for 30 min at room temperature, and rinsed with distilled water. For green fluorescence (SYTO 9, intact cells) excitation was performed at 488 nm and emission at 500–575 nm. For red fluorescence (PI, dead cells), the excitation/emission wavelengths were 561 nm and 570–620 nm respectively. For FilmTracer SYPRO Ruby staining the excitation/emission wavelengths were 450 nm and 610 nm respectively. SEM images of bacteria colonizing the surface of materials were taken in a ZEISS DSM-950 instrument using the same procedure described before for membrane performance images.

3. Results and Discussion

3.1. Electrospinning solutions

Several parameters influence the transformation of polymer solutions into electrospun nanofibers, which include, among others, viscosity, electrical conductivity, and the surface tension of the electrospinning solution [39]. The values of the viscosity and conductivity of the nanocrystals and electrospinning suspensions are shown in Table S1 (Supplementary material). The viscosity obtained for the solution containing PLA (core polymer) was 310.8 mPa s and that of PAN solution (shell polymer) 924.6 mPa s. The results showed that the addition of CNC_{H2SO4} and ChNC, induced a viscosity decrease in comparison with PAN solution, the lower viscosity corresponding to the more concentrated suspensions (20 wt%). A similar behavior was reported elsewhere [40–42]. After the addition of CNC_{BE}, however, viscosity increased due to the gel consistency of this nanocrystal solution. Compared with neat PLA core solution, the viscosity of the shell suspensions (PAN/NC) increased substantially.

The electrical conductivity of CNC (CNC_{H2SO4} and CNC_{BE}) was higher than that of ChNC as a consequence of their negatively charged surface groups like sulphate ester groups (resulting from sulfuric acid hydrolysis) and carboxyl groups [35]. The conductivity of ChNC suspensions was explained by the protonation of the N-H groups on chitin structure [37,43]. Increasing NC concentration there was a slight increase in electrical conductivity of the electrospinning suspensions.

3.2. Morphology of core/shell composite nanofibers

The stability of the core/shell structure of composite nanofibers is a consequence of the stability of the combined jet of two liquids, which in turn depends on their physical properties, feed rates and applied voltage [44,45]. In this work, the effect of interface tension was reduced using a similar solvent system for core and shell components, namely chloroform/DMF for the core and DMF for the shell. SEM micrographs of electrospun neat PLA and coaxial PAN/NC@PLA membranes are shown in Fig. 2(A–D) for the higher NC loadings Electrospun membranes were homogenous, exhibiting well defined, bead-free non-porous fibers. Fig. 2(E–H) also shows TEM images of PAN@PLA (E) and PAN/NC@PLA (F-H) core-shell composites for different NC loadings. The presence of nanocrystals on fiber surface is apparent. Further insight into fiber topography is shown in AFM images from Fig. S1. Accurate determination of NC on fiber surface was not possible from TEM images, but their dimensions were reported earlier. Nanocrystals had diameters in the range of 5–20 nm and length in the range of 100–300 nm, which agrees with the nanometer scale of the details observed in TEM images [28,35,37].

The average fiber diameters were 199 ± 52 nm for neat PLA, 339 ± 40 nm for PAN/CNC_{H2SO4}-20@PLA, 338 ± 35 nm for PAN/CNC_{BE}-20@PLA and 399 ± 37 nm for PAN/ChNC-20@PLA nanofibers. (The diameters for the rest of membranes are listed in Table S2). Fiber diameters and confidence intervals were obtained from at least 50 measurements in SEM micrographs. The diameter of coaxial PAN/NC@PLA fibers results from the structural organization of the composite fiber consisting of an inner core of PLA and an outer layer of PAN/NC. The diameter of coaxial fibers was higher for lower NC loadings, which can be explained in terms of the lower viscosity and higher conductivity of suspensions with higher NC contents [42,46]. The differences found in this work, however, were small and generally not significant.

Electrospinning produces highly porous nanofiber network structures with interconnected flow-through pores (Fig. 2). Bubble point test was performed to evaluate the opening size of the largest membrane pores. For pure PLA membranes, the largest mean pore size was 0.8 ± 0.1 μm, which increased for coaxial PAN@PLA membranes without nanocrystals to 1.2 ± 0.1 μm. Coaxial PAN/NC@PLA membranes displayed higher pore sizes, the largest values corresponding to membranes with higher NC loadings (Table S2). There were no significant differences for membranes with different types of NC at similar loadings.

3.3. Mechanical properties

The load-elongation curve was converted into a stress-strain plot according to Eqs. (2) and (3). Figs. 3–5 show the stress-strain curves of neat PLA and coaxial PAN/NC@PLA nanocomposite membranes. Table S2 gives the maximum tensile strength, σ_{max}, Young's modulus, E, and ultimate strain, ε, of all the membranes tested. Fig. 3 shows the curves for representative samples prepared with CNC_{H2SO4} and the corresponding matrices, PLA and PAN@PLA, while the average tensile data are shown in Table S2. For PLA membranes, the mean σ_{max} and E were 2.3 MPa and 0.51 GPa respectively in agreement with previously reported results [5,20,23,47]. Coaxial membranes with

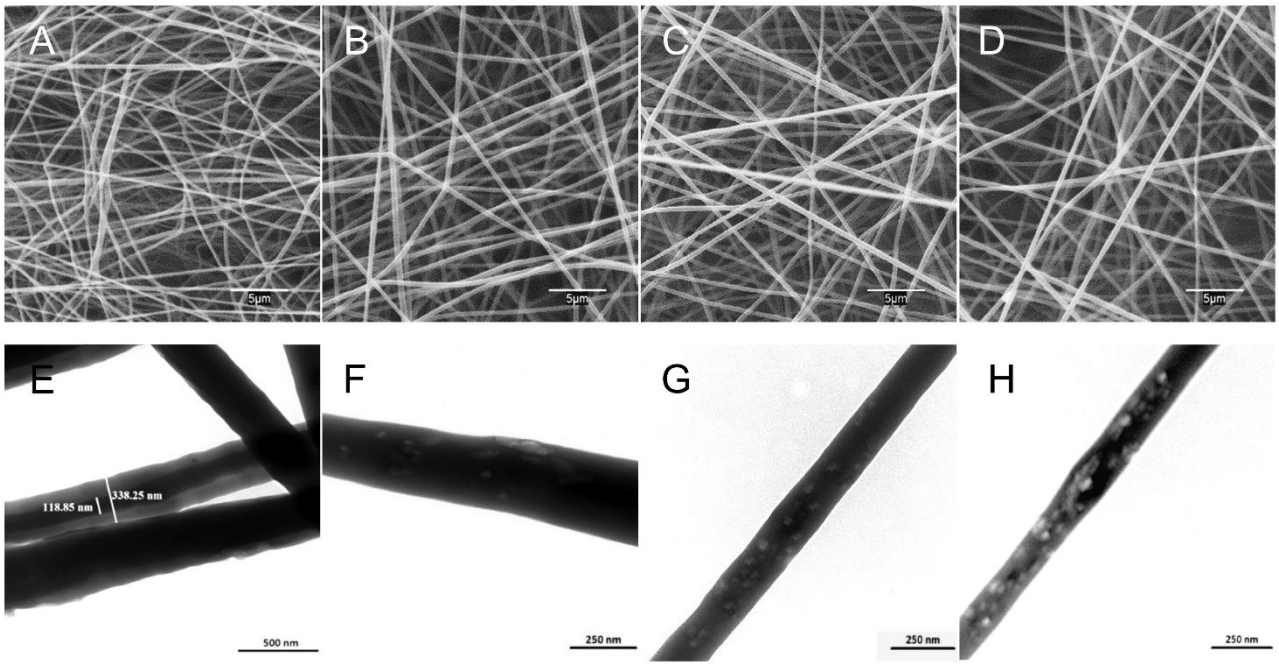

Figure 2. SEM micrographs of (A) neat PLA, (B) PAN/CNC_{H2SO4}- 20@PLA, (C) PAN/CNC_{BE}- 20@PLA, and (D) PAN/ChNC-20@PLA electrospun membranes. TEM images of (E) PAN@PLA core-shell fibers, (F), PAN/CNC_{H2SO4}-5@PLA, (G) PAN/CNC_{BE}-15@PLA, and (H) PAN/ChNC-20@PLA coaxial membranes showing NC on fiber surface.

CNC_{H2SO4} showed significant improvement in tensile strength at low NC content (5 wt%), which increased by 169% compared to the neat PLA membranes and by 260% compared to the coaxial membrane without NC, PAN@PLA. At 20 wt% CNC_{H2SO4}, the tensile properties of the coaxial nanocomposite membranes slightly decreased compared to neat PLA membranes, which could be attributed to the aggregation of NC at their high concentration levels on the fiber surface [48]. A similar trend was observed for Young's modules, PAN/CNC_{H2SO4}-5@PLA being the stiffest material with a 172 % increase respect to PLA and 146% respect to the coaxial membranes without NC.

Figs. 4 and 5 show the stress-strain curves for PLA and PAN/CNC_{BE}@PLA and PAN/ChNC@PLA coaxial membranes, the main parameters being presented in Table S2. Like CNC_{H2SO4} loaded membranes, coaxial membranes with 5 wt% CNC_{BE} were the strongest with an improvement in tensile strength of 188 % form neat PLA. Membranes loaded with 10% and 15% CNC_{BE} showed a slight decrease in $\sigma_{max,}$ which could be attributed to the irregular aligning and poor adhesion

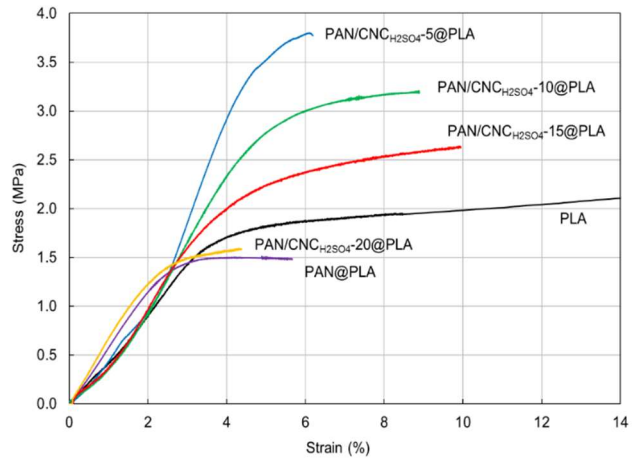

Figure 3. Stress-strain curves of PLA and PAN/CNC$_{H_2SO_4}$@PLA coaxial membranes.

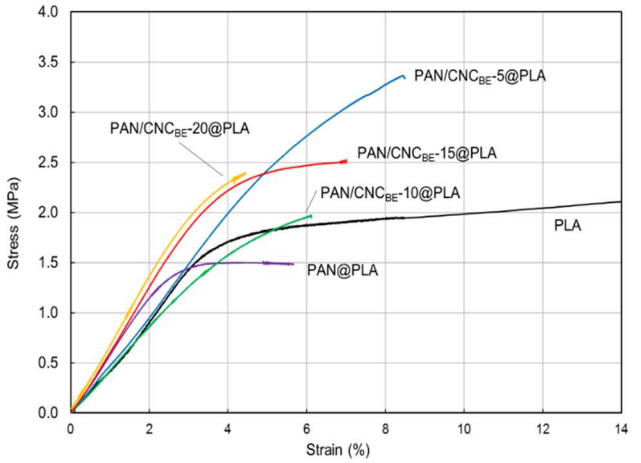

Figure 4. Stress-strain curves of PLA and PAN/CNC$_{BE}$@PLA coaxial membranes.

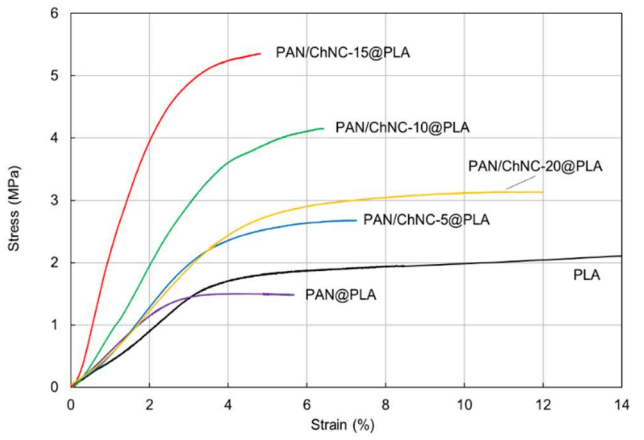

Figure 5. Stress-strain curves of PLA and PAN/ChNC@PLA coaxial membranes.

between fibers [49]. However, Young's modulus increased with higher NC content, being the 20 % CNC$_{BE}$ composition the stiffest, 176% over neat PLA membranes. All composite materials loaded with ChNC performed better than pure PLA and the coaxial PAN@PLA membranes, with best results for 15 wt% ChNC. Compared to PLA membranes, σ_{max} increased by 227 % and E by 529 % in PAN/ChNC-15@PLA composites, making these membranes the strongest and the stiffest among all tested specimens. The result agrees with previous studies that showed that chitin was able to improve the mechanical properties of electrospun cellulose acetate membranes by impregnation with ChNC [28].

Non-woven electrospun membranes are made of randomly oriented fibers and their mechanical properties depend on their direction and the interaction between fibers. The mechanical properties of electrospun membranes are given by the arrangement and packing characteristic of the nanofibers that made up the membrane. Poor adhesion between fibers and broad diameter distribution favor failure at the fiber-fiber interface and result in lower fiber strength [24]. Our results showed that coaxial PAN@PLA membranes displayed similar or lower values of Young's modulus and tensile strength than PLA (Table S2 and Figs. 3–5). We attributed this fact to a poorer adhesion between fibers in coaxial membranes, favoring failures at the fiber-fiber interface and bringing about lower mechanical strength. A higher solidification rate of PAN in comparison with PLA solution due to the higher polymer content and higher viscosity of PAN solutions, would result in fewer contact points and reduced cohesive force between fibers. The nonwoven membrane would then display a poorer mechanical performance [50]. The improvement in mechanical properties of coaxial nanocomposites of poly(ethylene oxide) electrospun fibers containing CNC has been attributed to the better stress transfer favored by nanocrystal alignment [24]. The enhancement of mechanical properties due to the incorporation of relatively low amounts of CNC fillers has been rationalized in terms of the mechanical percolation effect, due to the formation of a rigid interconnected structure of CNC [51]. The higher crystallinity induced by CNC has been also shown to result in harder and more thermally stable fibers [52]. The higher crystallinity of mixed PLA/CNC electrospun fibers arises from CNC acting as nucleation sites during the electrospinning of composite fibers [48].

The increase in Young's modulus of composite PLA membranes containing CNC was attributed to the smaller fiber diameter of composite materials as a consequence of the higher viscosity and electrical conductivity of PLA/CNC suspensions compared to neat PLA solutions [23]. For the coaxial composites prepared in this work the lower fiber diameter observed for membranes with higher NC loadings was not important enough to influence the mechanical properties of composite membranes. The improvement of Young's modulus of heterogeneous mats has also been related to the formation of secondary ultrafine nanofibers interacting with primary nanofibers through bonding points [24]. We also found the formation of secondary ultrafine nanofibers during the electrospinning of composite materials as shown in Fig. S2. Their formation is not probably extensive enough to significantly influence Young's modulus, but could

impact membrane size exclusion behavior as shown below.

Core-shell fibers have also been prepared using emulsion electrospinning with CNC forming the core and PLA the shell that showed strong structural reinforcing effect due to the formation of a rigid percolating network of CNC [53]. The membranes prepared in this work, with NC in the outer part of the fiber, displayed significantly enhanced mechanical properties due to the same reasons. For the three types of coaxial nanocomposites, the ultimate strain decreased compared to pure PLA membranes meaning that the coaxial structure and the presence of the nanocrystals reduced fiber ductility making membranes more resistant to deformation [54]. The decrease of the elongation of electrospun non-woven PLA fibers containing CNC was also reported for PLA/CNC non-coaxial nanocomposites as a consequence of the reinforcing effect [48].

3.4. Water flux and permeability

The permeability of electrospun PLA and PAN/NC@PLA coaxial membranes is shown in Fig. 6 and Table S2 for a transmembrane pressure of 0.2 bar. In all cases, the water flux was higher for the composite coaxial membranes than for neat PLA membranes (504 L m^{-2} h^{-1}) and for PAN@PLA coaxial membranes (777 L m^{-2} h^{-1}). PAN/CNC_{H2SO4}@PLA coaxial membranes displayed water fluxes increasing with CNC content from 1106 L m^{-2} h^{-1} (5 wt%) to 2140 L m^{-2} h^{-1} (20 wt%). Water flux for coaxial membranes coated with CNC_{BE} ranged from 1357 L m^{-2} h^{-1} (5 wt%) to 1700 L m^{-2} h^{-1} (20 wt%), while membranes with ChNC, which showed the highest flux values, ranged from 1403 L m^{-2} h^{-1} (5 wt%) to 2646 L m^{-2} h^{-1} (20 wt%). The incorporation of NC to the fiber surface increased pore size (Table S2) and significantly improved their wettability making them more hydrophilic (Table 2). Both factors explain the increased water flux and permeability observed in agreement with results published elsewhere on the effect of nanocellulose addition to polymeric membranes [55,56].

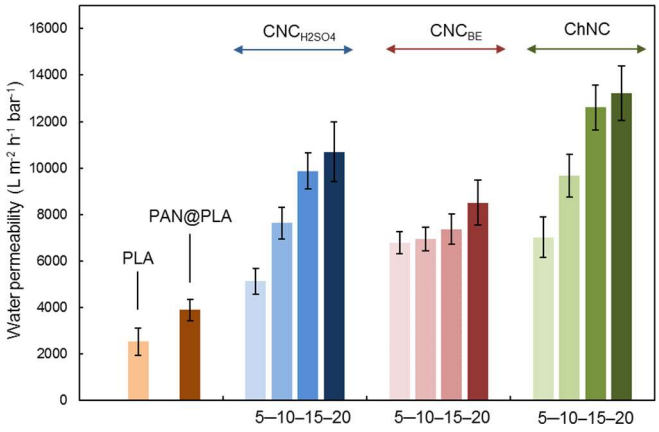

Figure 6. Water permeability of neat PLA and coaxial membranes.

3.5. Microfiltration evaluation

Suspensions of *E. coli* cells and *A. niger* spores, were used to evaluate the filtration performance of the developed composite coaxial membranes, which were chosen as representative for waterborne and airborne microorganism particles respectively. Fig. 7 shows that the efficiency of all the prepared membranes for the removal of bacterial cells and fungal spores. In all cases the removal efficiency increased in coaxial membranes with nanocrystals with respect to the pure polymeric membranes (PLA and PAN@PLA). The retention of

Table 2. Effect of nanocrystals on water contact angle, surface ζ-potential and biofilm formation[a].

Membranes	Water contact angle (WCA)	Surface ζ-potential (pH 7.5, mV)	FDA relative biofilm formation (18 h)
PLA	121.6 ± 2.4	-31.3 ± 3.9	1.00 ± 0.06
PAN@PLA	6.5 ± 3.2	-10.5 ± 1.3	2.94 ± 0.03
PAN/$CNC_{H_2SO_4}$-5@PLA	72.2 ± 3.6	-13.1 ± 4.0	3.68 ± 0.09
PAN/$CNC_{H_2SO_4}$-10@PLA	68.9 ± 2.5	-11.6 ± 2.1	5.19 ± 0.04
PAN/$CNC_{H_2SO_4}$-15@PLA	66 ± 1.8	-21.3 ± 1.7	5.87 ± 0.10
PAN/$CNC_{H_2SO_4}$-20@PLA	57.1 ± 4.1	-23.2 ± 3.0	7.67 ± 0.08
PAN/CNC_{BE}-5@PLA	80.8 ± 1.3	-13.8 ± 3.2	2.6 ± 0.2
PAN/CNC_{BE}-10@PLA	71.6 ± 2.1	-16.2 ± 2.9	4.2 ± 0.1
PAN/CNC_{BE}-15@PLA	64.9 ± 1.5	-23.6 ± 2.5	5.33 ± 0.07
PAN/CNC_{BE}-20@PLA	62 ± 2.3	-27.2 ± 3.3	6.68 ± 0.02
PAN/ChNC-5@PLA	0 [b]	-7.0 ± 1.8	0.31 ± 0.05
PAN/ChNC-10@PLA	0 [b]	-1.8 ± 2.4	0.21 ± 0.04
PAN/ChNC-15@PLA	0 [b]	0.7 ± 1.1	0.06 ± 0.15
PAN/ChNC-20@PLA	0 [b]	1.1 ± 2.1	0.02 ± 0.12

[a] ζ-potential measurements were performed at 25 °C using 10 mM KCl, pH 7.5, aqueous solution with 0.5 wt% poly(acrylic acid), for membranes negatively charged, and 0.5 wt% polyethylenimine, for membranes positively charged, as tracers.

[b] Too low to be measured.

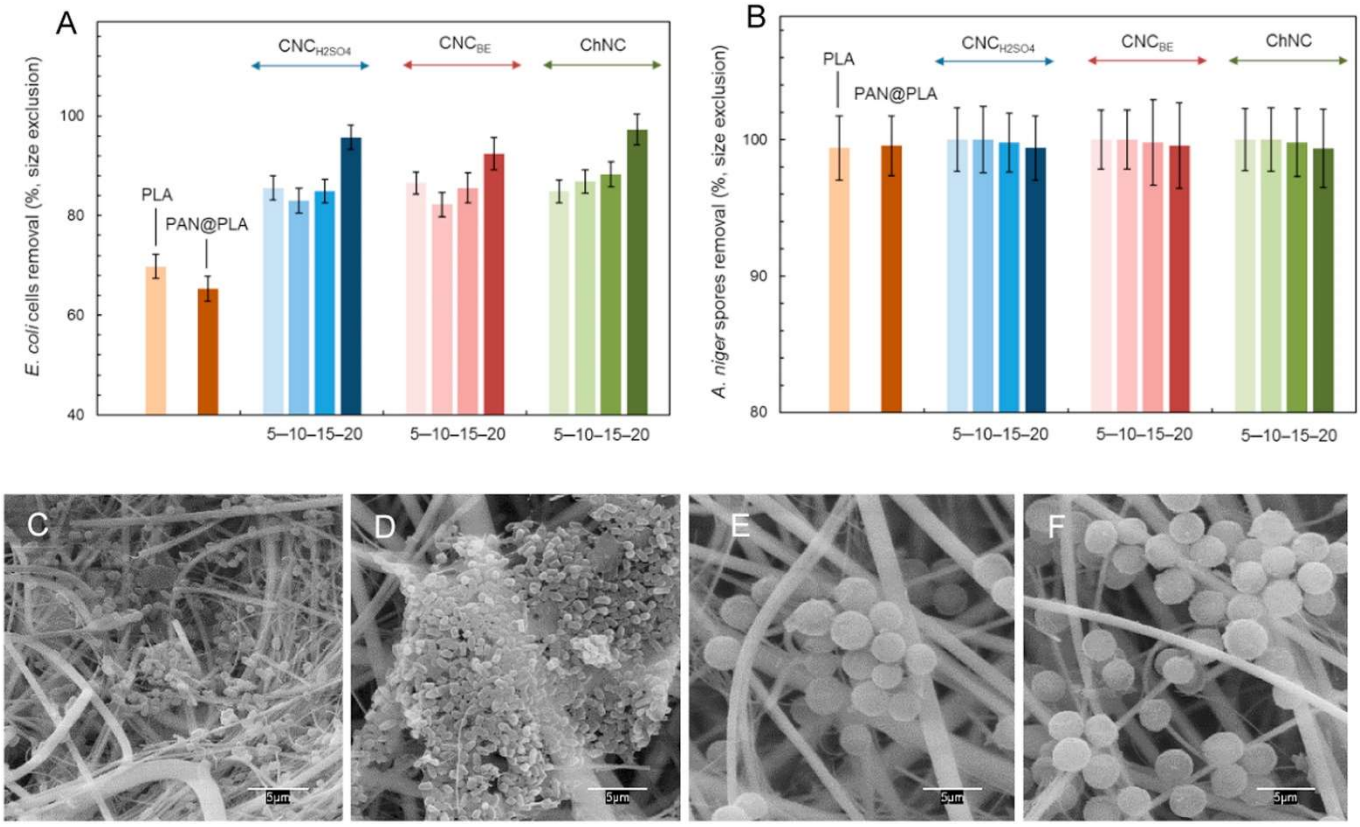

Figure 7. Size exclusion filtration efficiency for the removal of *E. coli* cells (A) and *A. niger* spores (B). SEM images of PAN/CNC$_{BE}$-15@PLA (C) and PAN/ChNC-20@PLA (D) coaxial membranes after filtering *E. coli* cells and SEM images of PAN/CNC$_{BE}$-20@PLA (E) and PAN/CNC$_{H2SO4}$-15@PLA (F) membranes after filtering *A. niger* spores. The numbers 5–10–15–20 correspond to the wt% of NC loading. (SEM images correspond to the same conditions shown in A-B; additional SEM images can be found in Fig. S3, SM).

bacteria increased from 70% (neat PLA membrane) and 65 % (PAN@PLA membrane) to values in the 85–98 % range. The results were in good agreement with the pore size of membranes as determined by the bubble point method. The latter is shown in Table S2 and was in the 1.2–2.6 μm range for all tested specimens, without significant differences among them (Table S2). The retention of *A. niger* spores was essentially complete, with removal values > 99% (not significantly different from 100%) for all membranes. The results were compatible with the expected size exclusion of the microfiltration membranes used in view of the size of the coliform bacteria (0.5 μm width × 2 μm length approx.) and *A. niger* spores, which range in size from 2 to 5 μm. Additionally, it has to be considered that the bubble point test cannot be used as the sole factor to describe the limiting size for retention of particulate material as the calculation is based on assuming cylindrical capillary pores. An additional factor is the elasticity of the fibers, which would allow better exclusion in the case of the more rigid membranes, as observed in this work.

Representative SEM images of selected membranes showing retained cells and spores are also included in Fig. 7 and for the rest of membranes in Fig. S3 (SM). A feature clearly observed in most SEM images is the network of secondary ultrafine nanofibers produced during the electrospinning of composite membranes, which may explain that the coaxial membranes with the highest NC loading were more efficient that the rest for the removal of bacterial cells. Similarly to other fibrous membranes, particles accumulated in the formed cake layer on membrane surface block open pores and allow rejecting particles higher than pore sizes, but this fouling layer decrease membrane permeability, increase transmembrane pressure and supposes a microbiological threat [57]. This aspect is being dealt with in detail in the following section.

3.6. Antimicrobial and antibiofilm performance

Microbial attachment during the initial steps of bacterial colonization are influenced by surface charge and hydrophobicity [15]. Surface hydrophilicity is given by the water contact angle (WCA) and the surface charge has been measured by surface ζ-potential. Table 2 shows the WCA and surface ζ-potential of the studied membranes. Neat PLA membranes were hydrophobic with WCA > 120°, while coaxial PAN@PLA membranes were highly hydrophilic, with WCA < 10°. Coaxial membranes with CNC$_{H2SO4}$ on the outer shell displayed WCA in the 57.1–72.2° range, similarly to those obtained with CNC$_{BE}$. In both cases, WCA decreased with increasing NC loadings and the more hydrophilic membranes corresponded to those loaded with 20% NC. Coaxial membranes prepared with ChNC showed superhydrophilicity with complete spreading of the water drop immediately after being deposited on the membrane. This is consistent with previous results

reported for coatings with chitin nanocrystals on the surface of cellulose acetate electrospun fibers [28]. Concerning surface charge, neat PLA membranes were negatively charged with ζ-potential of −31.3 ± 3.9 mV (pH 7.5), whereas coaxial PAN@PLA membranes displayed a surface ζ-potential of −10.5 ± 1.3 mV at the same pH. All coaxial membranes loaded with CNC (CNC_{H2SO4} and CNC_{BE}) were also negatively charged with surface ζ-potential ranging from −11.6 to −27.2 mV. Surface ζ-potential values were more negative for increased NC contents and slightly more negative in the case of CNC_{BE}. PAN/ChNC@PLA membranes were negatively charged for low NC loadings turning neutral or positive for the higher ChNC contents. The chemical structure of the nanocrystals on the surface of the polymeric coaxial fibers influenced membrane surface properties making them more hydrophilic and less negatively charged. The carboxyl groups in CNC_{BE} and CNC_{H2SO4}, more abundant in the former, explain the negative charge of membranes [35]. Chitin nanocrystals possess amino groups due to acid hydrolysis-induced deacetylation, the protonation of which makes the surface overall less negative or even positively charged surface charge [37,58].

Fig. 8 shows the confocal images for Live/Dead bacterial viability (A, C, E and G) and Ruby FilmTracer staining (B, D, F and H). Regarding bacterial viability, PLA and CNC did not significantly impair bacterial cells, as noted by the absence of red-marked (cell membrane-damaged) bacteria in Fig. 8A, C and E. Conversely, chitin nanocrystals remarkably reduced the viability of the cells on membrane surface as shown by the high number of PI-marked non-viable cells on

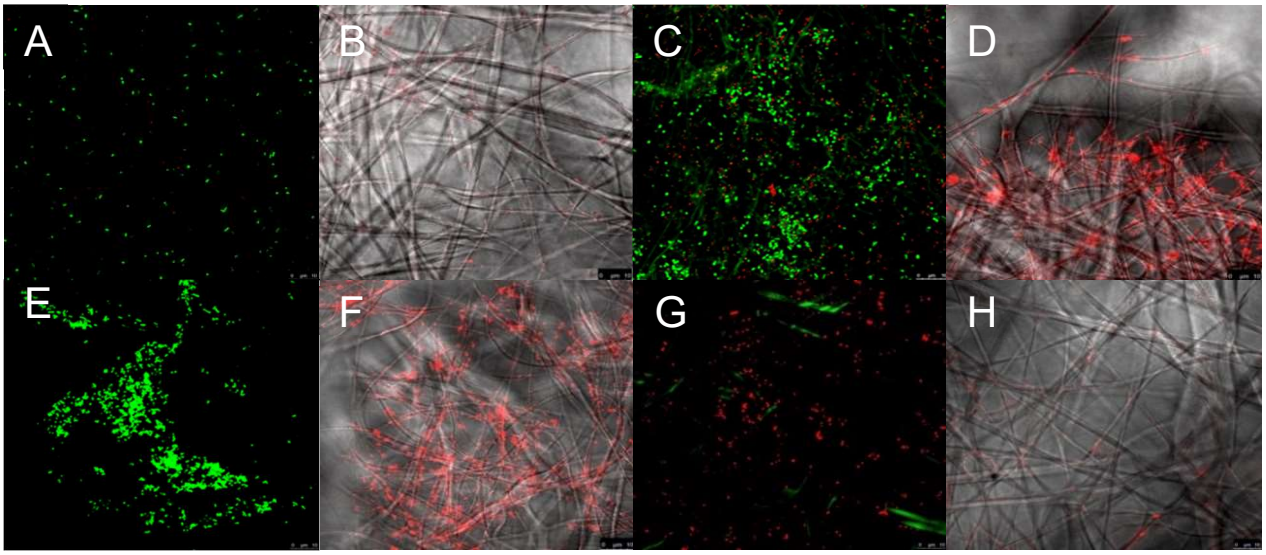

Figure 8. Live/Dead double staining (A, C, E and G) and FilmTracer SYPRO Ruby biofilm matrix staining (B, D, F and H) of *E. coli* on membranes of PLA (A and B), PAN/CNC_{H2SO4}-20@PLA (C and D), PAN/CNC_{BE}-20@PLA (E and F) and PAN/ChNC-20@PLA (G and H) after 18 h of biofilm incubation. Live cells were green stained by SYTO 9 and dead cells were red stained by PI (A, C, E and G).

PAN/ChNC@PLA membranes (Fig. 8G). The antibacterial effect of natural chitin is believed to arise from a small portion of deacetylated structural units in their chitin structure [59]. The acid hydrolysis produced during the extraction of nanocrystals enlarges the proportion of deacetylated groups with the outcome of a high antibacterial activity [60,61]. The hydrolytic treatment leads to the formation of NH_3^+ groups, which can interact with the negatively charged residues of carbohydrates, lipids and proteins located on the cell surface of bacteria, so explaining their role in bacterial impairment [58,62].

Fig. 9 shows SEM micrographs of membranes kept in contact with *E. coli* cultures for 18 h. PLA membranes displayed moderated resistance to be colonized by *E. coli* (Fig. 9A) with very reduced poor protein network of extracellular matrix indicating low biofilm formation (Fig. 8B). These observations agree with the enzymatic activity collected from FDA staining (Table 2). The coaxial membranes loaded with CNC, however, presented an important development of the extracellular matrix and biofilm formation upon contact with *E. coli* cultures (Fig. 8D and F and Fig. 9B and C). No significant differences in the susceptibility to *E. coli* colonization was observed between CNC_{H2SO4} and CNC_{BE}, but higher NC loadings led to increased microbial colonization as shown in the FDA values of Table 2. However, coaxial membranes prepared with ChNC presented significant resistance to bacterial colonization and biofilm formation (Fig. 8G and H and Fig. 9D and Table 2).

Our results showed that bacterial colonization took place preferentially on membranes with intermediate hydrophilicity values, whereas the more hydrophobic (PLA) and the more hydrophilic (PAN@PLA) surfaces presented a lower affinity for bacteria as shown by

FDA enzymatic activity (Table 2). This result is consistent with previously reported data concerning the attachment of a hydrophilic *E. coli* strain to glass-like carbon films [63]. Other studies reported that microorganisms preferably attach to hydrophobic nonpolar surfaces rather than to hydrophilic materials [64,65]. There is no general conclusion on the rationalization of bacterial attachment to surfaces exclusively in terms of hydrophilic-hydrophobic interactions at least due to two reasons. First, cell binding is affected by the culture media used due to differences in surface tension or the absorption of organic and inorganic compounds, which modify the way microorganisms adhere [66]. Second, bacterial morphology complicates cell-surface interactions due to the existence of cell appendages and adhesion structures avoiding direct contact [67].

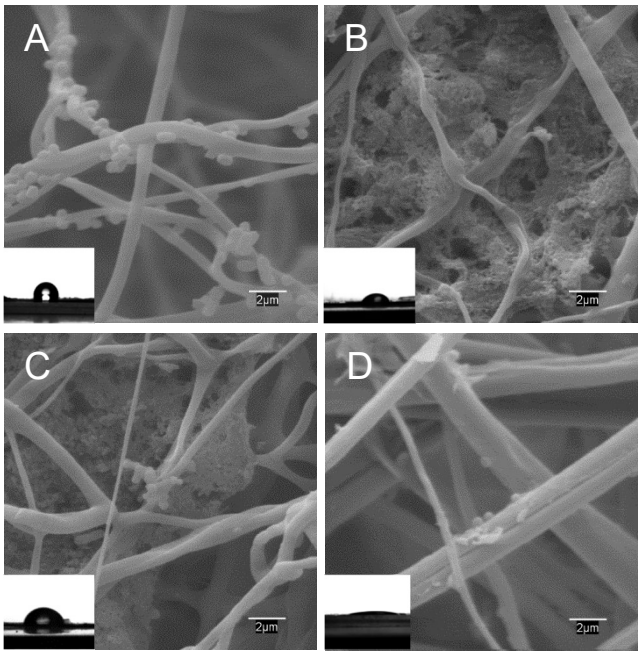

Figure 9. SEM images of *E. coli* colonization of PLA membranes (A), PAN/CNC_{H2SO4}-20@PLA (B), PAN/CNC_{BE}-20@PLA (C), and PAN/ChNC-20@PLA (D) after 18 h of biofilm incubation.

The other general factor governing bacterial adhesion is surface charge. The overall surface charge of bacterial outer membranes is negative, the ζ-potential of *E. coli* being about −30 mV [64]. Therefore, given the negative surface charge of the CNC membranes used in this study, the electrostatic repulsion could be expected to avoid colonization. However, the data showed that the negatively charged surfaces of CNC-loaded membranes displayed higher bacterial colonization and biofilm formation than PAN@PLA membranes. A combination of hydrophilic interaction and the fact that cells bearing an overall negative charge, also possess positively charged domains, which could interact with negatively charged surfaces, could explain results like those obtained in this work [68,69]. On the other hand, the neutral of more charged and superhydrophilic surfaces of PAN/ChNC@PLA composites were actually resistant to bacterial colonization. These results suggest that the high hydrophilicity of membranes with ChNC together with the presence of positively charged groups able to impair cell membranes would be the factors explaining the low bacterial colonization and biofilm formation of PAN/ChNC@PLA membranes.

Coaxial PAN/ChNC@PLA membranes combine improved mechanical properties, an increase in water flux and permeability and a noteworthy antimicrobial behavior. It is significant that the incorporation of CNC confers similar mechanical and filtration properties but a much poorer performance in terms of antibiofouling resistance. This would be a significant advantage for applications in which biofilm formation is undesirable. Conversely, enhanced formation of biofilms would favor applications in which the microbial communities in the biofilm are pursued. For example, for the design of biofilters.

4. Conclusions

Core-shell nanocomposite membranes were prepared by coaxial electrospinning. Cellulose or chitin nanocrystals were electrospun with PAN to create the outer layer of core-shell fibers, the inner part of which was PLA. The membranes consisted of an homogeneous layer of non-woven well-defined fibers with external diameter in the 350–400 nm range and inner core > 100 nm.

The mechanical properties of composite membranes significantly enhanced upon incorporation of 5–20 wt% of NC, reaching ultimate tensile strength like that of non-coaxial PLA fibers. Best results concerning tensile strength and Young's modulus were obtained for 5 wt% CNC and 15 wt% ChNC-loadings. The reinforcing effect was attributed to the percolating network of nanocrystals.

The incorporation of NC significantly enhanced water flux. Permeability increased by at least a factor of two for membranes with 20 wt% NC with respect to coaxial PAN@PLA without NC. Pore size was in the 1.2–2.6 μm range for all coaxial membranes, and proved suitable for microfiltration applications. All NC-loaded membranes blocked *A. niger* spores > 99% and retained > 85% of *E. coli* cells by size exclusion, with best results for ChNC loaded coaxials (> 95% *E. coli* rejection).

The incorporation of NC to the outer layer of coaxial fibers made membranes more hydrophilic and less negatively charged than PLA. In the case of ChNC composites the membranes displayed superhydrophilicity and neutral or slightly positive surface charge. The coaxial membranes containing ChNC were much less prone to microbial colonization and were essentially free of biofilm formation after exposure to *E. coli* cultures in conditions strongly favoring microbial growth. The results showed

extensive cell impairment for bacteria in contact with membrane surface.

Acknowledgements

Financial support for this work was provided by the FP7-ERA-Net Susfood, 2014/00153/001, the Spanish Ministry of Economy and Competitiveness, CTM2013-45775 and the Regional Government of Madrid through program S2013/MAE-2716. APM acknowledges Luleå University of Technology for providing access to mechanical testing equipment.

References

[1] N. Bhardwaj, S.C. Kundu, Electrospinning: A fascinating fiber fabrication technique, Biotechnology Advances, 28 (2010) 325-347.

[2] W.E. Teo, S. Ramakrishna, A review on electrospinning design and nanofibre assemblies, Nanotechnology, 17 (2006) R89.

[3] L. Persano, A. Camposeo, C. Tekmen, D. Pisignano, Industrial upscaling of electrospinning and applications of polymer nanofibers: a review, Macromolecular Materials and Engineering, 298 (2013) 504-520.

[4] F.E. Ahmed, B.S. Lalia, R. Hashaikeh, A review on electrospinning for membrane fabrication: Challenges and applications, Desalination, 356 (2015) 15-30.

[5] L. Li, R. Hashaikeh, H.A. Arafat, Development of eco-efficient micro-porous membranes via electrospinning and annealing of poly (lactic acid), Journal of Membrane Science, 436 (2013) 57-67.

[6] S. Kaur, S. Sundarrajan, D. Rana, R. Sridhar, R. Gopal, T. Matsuura, S. Ramakrishna, Review: the characterization of electrospun nanofibrous liquid filtration membranes, Journal of Materials Science, 49 (2014) 6143-6159.

[7] J. Yao, C. Bastiaansen, T. Peijs, High strength and high modulus electrospun nanofibers, Fibers, 2 (2014) 158.

[8] X. Wang, K. Zhang, M. Zhu, B.S. Hsiao, B. Chu, Enhanced Mechanical Performance of Self-Bundled Electrospun Fiber Yarns via Post-Treatments, Macromolecular Rapid Communications, 29 (2008) 826-831.

[9] J.S. Jeong, J.S. Moon, S.Y. Jeon, J.H. Park, P.S. Alegaonkar, J.B. Yoo, Mechanical properties of electrospun PVA/MWNTs composite nanofibers, Thin Solid Films, 515 (2007) 5136-5141.

[10] A. Doustgani, E. Vasheghani-Farahani, M. Soleimani, S. Hashemi-Najafabadi, Optimizing the mechanical properties of electrospun polycaprolactone and nanohydroxyapatite composite nanofibers, Composites Part B: Engineering, 43 (2012) 1830-1836.

[11] V. Kochkodan, N. Hilal, A comprehensive review on surface modified polymer membranes for biofouling mitigation, Desalination, 356 (2015) 187-207.

[12] P. Zhang, L. Lin, D. Zang, X. Guo, M. Liu, Designing bioinspired anti-biofouling surfaces based on a superwettability strategy, Small, (2016) n/a-n/a.

[13] H.C. Flemming, Biofouling in water systems – cases, causes and countermeasures, Applied Microbiology and Biotechnology, 59 (2002) 629-640.

[14] D. Rana, T. Matsuura, Surface modifications for antifouling membranes, Chemical Reviews, 110 (2010) 2448-2471.

[15] T.R. Garrett, M. Bhakoo, Z. Zhang, Bacterial adhesion and biofilms on surfaces, Progress in Natural Science, 18 (2008) 1049-1056.

[16] C.D. Nadell, K. Drescher, K.R. Foster, Spatial structure, cooperation and competition in biofilms, Nature Reviews Microbiology, 14 (2016) 589-600.

[17] J. Quirós, K. Boltes, S. Aguado, R. Guzman de Villoria, J.J. Vilatela, R. Rosal, Antimicrobial metal-organic frameworks incorporated into electrospun fibers, Chemical Engineering Journal, 262 (2015) 189-197.

[18] S. Torres-Giner, M.J. Ocio, J.M. Lagarón, Novel antimicrobial ultrathin structures of zein/chitosan blends obtained by electrospinning, Carbohydrate Polymers, 77 (2009) 261-266.

[19] C. Yao, X.S. Li, K.G. Neoh, Z.L. Shi, E.T. Kang, Surface modification and antibacterial activity of electrospun polyurethane fibrous membranes with quaternary ammonium moieties, Journal of Membrane Science, 320 (2008) 259-267.

[20] A. Moriya, T. Maruyama, Y. Ohmukai, T. Sotani, H. Matsuyama, Preparation of poly(lactic acid) hollow fiber membranes via phase separation methods, Journal of Membrane Science, 342 (2009) 307-312.

[21] D. Klemm, F. Kramer, S. Moritz, T. Lindstrom, M. Ankerfors, D. Gray, A. Dorris, Nanocelluloses: A new family of nature-based materials, Angewandte Chemie-International Edition, 50 (2011) 5438-5466.

[22] R.J. Moon, A. Martini, J. Nairn, J. Simonsen, J. Youngblood, Cellulose nanomaterials review: structure, properties and nanocomposites, Chemical Society Reviews, 40 (2011) 3941-3994.

[23] Q.F. Shi, C.J. Zhou, Y.Y. Yue, W.H. Guo, Y.Q. Wu, Q.L. Wu, Mechanical properties and in vitro degradation of electrospun bio-nanocomposite mats from PLA and cellulose nanocrystals, Carbohydrate Polymers, 90 (2012) 301-308.

[24] C.J. Zhou, R. Chu, R. Wu, Q.L. Wu, Electrospun polyethylene oxide/cellulose nanocrystal composite nanofibrous mats with homogeneous and heterogeneous microstructures, Biomacromolecules, 12 (2011) 2617-2625.

[25] C.J. Zhou, Q.L. Wu, Y.Y. Yue, Q.G. Zhang, Application of rod-shaped cellulose nanocrystals in polyacrylamide hydrogels, Journal of Colloid and Interface Science, 353 (2011) 116-123.

[26] M. Mincea, A. Negrulescu, V. Ostafe, Preparation, modification and applications of chitin nanowhiskers: A review, Reviews on Advanced Materials Science, 30 (2012) 225-242.

[27] A.W. Qin, X. Li, X.Z. Zhao, D.P. Liu, C.J. He, Preparation and characterization of nano-chitin whisker reinforced PVDF membrane with excellent antifouling property, Journal of Membrane Science, 480 (2015) 1-10.

[28] L.A. Goetz, B. Jalvo, R. Rosal, A.P. Mathew, Superhydrophilic anti-fouling electrospun cellulose acetate membranes coated with chitin nanocrystals for water filtration, Journal of Membrane Science, 510 (2016) 238-248.

[29] C. Xiang, Y.L. Joo, M.W. Frey, Nanocomposite fibers electrospun from poly(lactic acid)/cellulose

nanocrystals, Journal of Biobased Materials and Bioenergy, 3 (2009) 147-155.
[30] Q. Shi, C. Zhou, Y. Yue, W. Guo, Y. Wu, Q. Wu, Mechanical properties and in vitro degradation of electrospun bio-nanocomposite mats from PLA and cellulose nanocrystals, Carbohydrate Polymers, 90 (2012) 301-308.
[31] S. Pirani, H.M.N. Abushammala, R. Hashaikeh, Preparation and characterization of electrospun PLA/nanocrystalline cellulose-based composites, Journal of Applied Polymer Science, 130 (2013) 3345-3354.
[32] C. López de Dicastillo, L. Garrido, N. Alvarado, J. Romero, J.L. Palma, M.J. Galotto, Improvement of polylactide properties through cellulose nanocrystals embedded in poly(vinyl alcohol) electrospun nanofibers, Nanomaterials, 7 (2017) 106.
[33] D. Bondeson, A. Mathew, K. Oksman, Optimization of the isolation of nanocrystals from microcrystalline cellulose by acid hydrolysis, Cellulose, 13 (2006) 171-180.
[34] K. Oksman, J.A. Etang, A.P. Mathew, M. Jonoobi, Cellulose nanowhiskers separated from a bio-residue from wood bioethanol production, Biomass & Bioenergy, 35 (2011) 146-152.
[35] A.P. Mathew, K. Oksman, Z. Karim, P. Liu, S.A. Khan, N. Naseri, Process scale up and characterization of wood cellulose nanocrystals hydrolysed using bioethanol pilot plant, Industrial Crops and Products, 58 (2014) 212-219.
[36] K.G. Nair, A. Dufresne, Crab shell chitin whisker reinforced natural rubber nanocomposites. 1. Processing and swelling behavior, Biomacromolecules, 4 (2003) 657-665.
[37] A.P. Mathew, M.P.G. Laborie, K. Oksman, Cross-linked chitosan/chitin crystal nanocomposites with improved permeation selectivity and pH stability, Biomacromolecules, 10 (2009) 1627-1632.
[38] S.K. Tiwari, S.S. Venkatraman, Importance of viscosity parameters in electrospinning: Of monolithic and core–shell fibers, Materials Science and Engineering: C, 32 (2012) 1037-1042.
[39] J. Doshi, D.H. Reneker, Electrospinning process and applications of electrospun fibers, Journal of Electrostatics, 35 (1995) 151-160.
[40] N. Naseri, C. Algan, V. Jacobs, M. John, K. Oksman, A.P. Mathew, Electrospun chitosan-based nanocomposite mats reinforced with chitin nanocrystals for wound dressing, Carbohydrate Polymers, 109 (2014) 7-15.
[41] N. Naseri, A.P. Mathew, L. Girandon, M. Frohlich, K. Oksman, Porous electrospun nanocomposite mats based on chitosan-cellulose nanocrystals for wound dressing: effect of surface characteristics of nanocrystals, Cellulose, 22 (2015) 521-534.
[42] N. Naseri, A.P. Mathew, K. Oksman, Electrospinnability of bionanocomposites with high nanocrystal loadings: The effect of nanocrystal surface characteristics, Carbohydrate Polymers, 147 (2016) 464-472.
[43] P.M. Shyly, S.D.D. Roy, P. Thiravetyan, S. Thanikaikarasan, P.J. Sebastian, D. Eapen, X.S. Shajan, Investigations on the effect of chitin nanofiber in PMMA based solid polymer electrolyte systems, Journal of New Materials for Electrochemical Systems, 17 (2014) 147-152.
[44] I.G. Loscertales, A. Barrero, I. Guerrero, R. Cortijo, M. Marquez, A.M. Ganan-Calvo, Micro/nano encapsutation via electrified coaxial liquid jets, Science, 295 (2002) 1695-1698.
[45] J.E. Díaz, A. Barrero, M. Márquez, I.G. Loscertales, Controlled encapsulation of hydrophobic liquids in hydrophilic polymer nanofibers by co-electrospinning, Advanced Functional Materials, 16 (2006) 2110-2116.
[46] X.H. Zong, K. Kim, D.F. Fang, S.F. Ran, B.S. Hsiao, B. Chu, Structure and process relationship of electrospun bioabsorbable nanofiber membranes, Polymer, 43 (2002) 4403-4412.
[47] R.A. Auras, L.T. Lim, S.E.M. Selke, H. Tsuji, Poly(lactic acid): synthesis, structures, properties, processing, and applications, John Wiley & Sons, 2011.
[48] C. Xiang, Y.L. Joo, M.W. Frey, Nanocomposite fibers electrospun from poly (lactic acid)/cellulose nanocrystals, Journal of Biobased Materials and Bioenergy, 3 (2009) 147-155.
[49] M.S. Huda, L.T. Drzal, A.K. Mohanty, M. Misra, Effect of fiber surface-treatments on the properties of laminated biocomposites from poly (lactic acid)(PLA) and kenaf fibers, Composites Science and Technology, 68 (2008) 424-432.
[50] X.J. Han, B.J. Cheng, Y.J. Li, Z.M. Huang, C. Huang, Z.F. Du, J. Wang, The effects of electrospinning parameters on coaxial polyacrylonitrile/polyurethane nanofibers: Morphology and water vapour transmission rate, Fibers and Polymers, 16 (2015) 2237-2243.
[51] S. Huan, L. Bai, G. Liu, W. Cheng, G. Han, Electrospun nanofibrous composites of polystyrene and cellulose nanocrystals: manufacture and characterization, RSC Advances, 5 (2015) 50756-50766.
[52] A. El-Hadi, R. Schnabel, E. Straube, G. Müller, S. Henning, Correlation between degree of crystallinity, morphology, glass temperature, mechanical properties and biodegradation of poly (3-hydroxyalkanoate) PHAs and their blends, Polymer Testing, 21 (2002) 665-674.
[53] Y. Li, F.K. Ko, W.Y. Hamad, Effects of emulsion droplet size on the structure of electrospun ultrafine biocomposite fibers with cellulose nanocrystals, Biomacromolecules, 14 (2013) 3801-3807.
[54] J. Lee, G. Tae, Y.H. Kim, I.S. Park, S.H. Kim, S.H. Kim, The effect of gelatin incorporation into electrospun poly (l-lactide-co-ε-caprolactone) fibers on mechanical properties and cytocompatibility, Biomaterials, 29 (2008) 1872-1879.
[55] H. Ma, C. Burger, B.S. Hsiao, B. Chu, Nanofibrous microfiltration membrane based on cellulose nanowhiskers, Biomacromolecules, 13 (2011) 180-186.
[56] P. Qu, H. Tang, Y. Gao, L. Zhang, S. Wang, Polyethersulfone composite membrane blended with cellulose fibrils, BioResources, 5 (2010) 2323-2336.
[57] R. Wang, Y. Liu, B. Li, B.S. Hsiao, B. Chu, Electrospun nanofibrous membranes for high flux microfiltration, Journal of Membrane Science, 392 (2012) 167-174.

[58] A. Mera, J. Araki, T. Ohtsuki, M. Shimosaka, N. Yoshida, Chitin nanowhiskers mediate transformation of *Escherichia coli* by exogenous plasmid DNA, Journal of Biotechnology and Biomaterials, 1 (2011).
[59] C. Peniche, W. Argüelles-Monal, F. Goycoolea, Chitin and chitosan: major sources, properties and applications, Monomers, polymers and composites from renewable resources, 1 (2008) 517-542.
[60] M.S. Benhabiles, R. Salah, H. Lounici, N. Drouiche, M.F.A. Goosen, N. Mameri, Antibacterial activity of chitin, chitosan and its oligomers prepared from shrimp shell waste, Food Hydrocolloids, 29 (2012) 48-56.
[61] W. Tachaboonyakiat, E. Sukpaiboon, O. Pinyakong, Development of an antibacterial chitin betainate wound dressing, Polymer Journal, 46 (2014) 505-510.
[62] Y. Andres, L. Giraud, C. Gerente, P. Le Cloirec, Antibacterial effects of chitosan powder: mechanisms of action, Environmental Technology, 28 (2007) 1357-1363.
[63] B. Jalvo, J. Santiago-Morales, P. Romero, R. Guzman de Villoria, R. Rosal, Microbial colonisation of transparent glass-like carbon films triggered by a reversible radiation-induced hydrophobic to hydrophilic transition, RSC Advances, 6 (2016) 50278-50287.
[64] Y.L. Ong, A. Razatos, G. Georgiou, M.M. Sharma, Adhesion Forces between *E. coli* bacteria and biomaterial surfaces, Langmuir, 15 (1999) 2719-2725.
[65] B. Prakash, B. Veeregowda, G. Krishnappa, Biofilms: a survival strategy of bacteria, Current Science, 85 (2003) 1299-1307.
[66] C.J. van Oss, Hydrophobicity and hydrophilicity of biosurfaces, Current Opinion in Colloid & Interface Science, 2 (1997) 503-512.
[67] K. Hori, S. Matsumoto, Bacterial adhesion: from mechanism to control, Biochemical Engineering Journal, 48 (2010) 424-434.
[68] A. Dasari, J. Quirós, B. Herrero, K. Boltes, E. García-Calvo, R. Rosal, Antifouling membranes prepared by electrospinning polylactic acid containing biocidal nanoparticles, Journal of Membrane Science, 405 (2012) 134-140.
[69] C. Wilhelm, C. Billotey, J. Roger, J. Pons, J.-C. Bacri, F. Gazeau, Intracellular uptake of anionic superparamagnetic nanoparticles as a function of their surface coating, Biomaterials, 24 (2003) 1001-1011.

Supplementary Material

Coaxial poly(lactic acid) electrospun composite membranes incorporating cellulose and chitin nanocrystals

Blanca Jalvo[1], Aji P. Mathew[2,*], Roberto Rosal[1,*]

[1] Department of Chemical Engineering, University of Alcalá, E-28871 Alcalá de Henares, Madrid, Spain
[2] Department of Materials and Environmental Chemistry, Stockholm University, Stockholm, Sweden

* Corresponding authors: mfaraldos@icp.csic.es, roberto.rosal@uah.es

CONTENTS:

Table S1. Viscosity and electrical conductivity of raw nanocrystal and electrospinning suspensions.

	Viscosity (mPa s)	Electrical conductivity ($\mu S\ cm^{-1}$)
CNC_{H2SO4} (1.3 wt%)	1.06	1764
CNC_{BE} (1.5 wt%)	1112	1895
ChNC (0.5 wt%)	0.95	721.1
PLA (7 wt% in $CHCl_3$/DMF, 3:2 vol.)	310.8	1.4
PAN (10 wt% DMF)	924.6	55.0
PAN/CNC_{H2SO4} 5%	834.4	67.5
PAN/CNC_{H2SO4} 10%	716.1	62.9
PAN/CNC_{H2SO4} 15%	628.9	71.3
PAN/CNC_{H2SO4} 20%	597.8	77.4
PAN/CNC_{BE} 5%	1037	70.0
PAN/CNC_{BE} 10%	1221	70.1
PAN/CNC_{BE} 15%	1374	75.7
PAN/CNC_{BE} 20%	1450	83.2
PAN/ChNC 5%	851.0	59.6
PAN/ChNC 10%	764.1	56.8
PAN/ChNC 15%	622.4	62.9
PAN/ChNC 20%	598.2	65.5

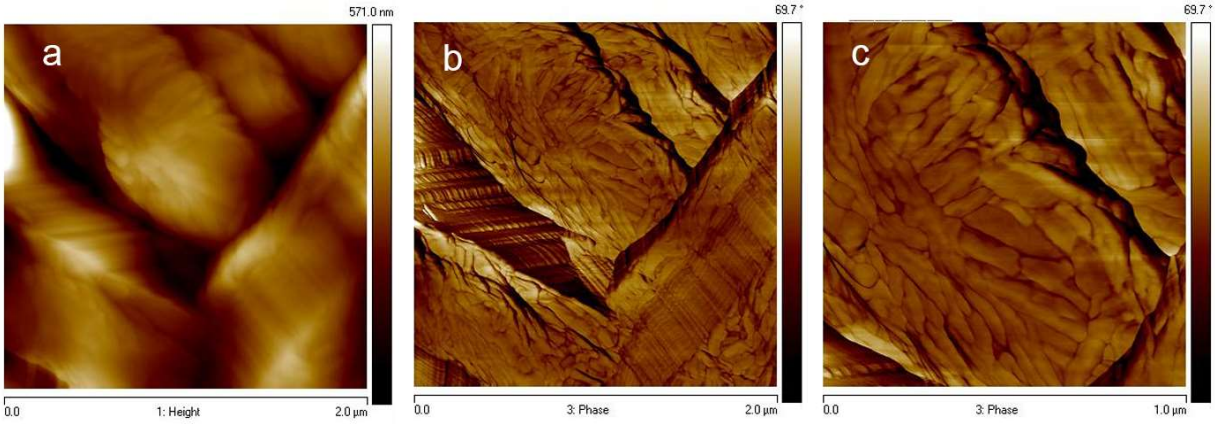

Figure S1. AFM images showing height (a) and phase images (b, c) of PAN/CNC_{AC}-20@PLA fibers at 2 x 2 µm (a, b) and 1 x 1 µm (c) magnifications.

Table S2. Fiber diameter, maximum pore size, mechanical properties, water flux and permeability of membranes.

	PLA	PAN@PLA	PAN/CNC_{AH}-5@PLA	PAN/CNC_{AH}10@PLA	PAN/CNC_{AH}-15@PLA	PAN/CNC_{AH}-20@PLA
Fiber diameter, nm	199 ± 52	458 ± 31	360 ± 25	356 ± 18	349 ± 29	339 ± 40
Max. pore size, μm	0.8 ± 0.1	1.2 ± 0.1	1.3 ± 0.1	1.5 ± 0.1	2.1 ± 0.1	2.5 ± 0.1
Tensile strength, MPa	2.4 ± 0.5	1.5 ± 0.3	3.9 ± 1.1	3.2 ± 0.9	2.9 ± 0.4	2.0 ± 0.3
Strain, %	17.9 ± 1.7	5.5 ± 1.0	6.2 ± 0.7	8.9 ± 1.5	9.9 ± 1.2	4.4 ± 0.9
Young's modulus, GPa	0.5 ± 0.1	0.6 ± 0.1	0.9 ± 0.1	0.7 ± 0.1	0.7 ± 0.1	0.7 ± 0.1
Flux, L m^{-2} h^{-1}	504 ± 32	777 ± 37	1106 ± 50	1472 ± 40	1875 ± 33	2140 ± 12
Permeability, L m^{-2} h^{-1} bar^{-1}	2024 ± 55	3888 ± 86	5531 ± 150	7634 ± 178	9375 ± 166	10701 ± 60

	PAN/CNC_{BE}-5@PLA	PAN/CNC_{BE}-10@PLA	PAN/CNC_{BE}-15@PLA	PAN/CNC_{BE}-20@PLA
Fiber diameter, nm	356 ± 34	351 ± 17	342 ± 23	338 ± 35
Max. pore size, μm	1.2 ± 0.1	1.5 ± 0.1	2.2 ± 0.12	2.6 ± 0.1
Tensile strength, MPa	4.4 ± 1.4	1.8 ± 0.5	1.5 ± 1.3	2.4 ± 0.1
Strain, %	16.9 ± 1.9	5.1 ± 1.1	5.7 ± 1.0	4.4 ± 0.9
Young's modulus, GPa	0.5 ± 0.1	0.5 ± 0.1	0.9 ± 0.1	0.9 ± 0.1
Flux, L m^{-2} h^{-1}	1357 ± 74	1390 ± 23	1472 ± 29	1700 ± 53
Permeability, L m^{-2} h^{-1} bar^{-1}	6788 ± 171	6952 ± 114	7365 ± 147	8503 ± 167

	PAN/ChNC-5@PLA	PAN/ChNC-10@PLA	PAN/ChNC-15@PLA	PAN/ChNC-20@PLA
Fiber diameter, nm	422 ± 26	415 ± 13	409 ± 21	399 ± 37
Max. pore size, μm	1.3 ± 0.1	1.6 ± 0.1	2.1 ± 0.1	2.5 ± 0.1
Tensile strength, MPa	2.7 ± 0.6	4.1 ± 0.7	5.4 ± 0.2	2.9 ± 1.0
Strain, %	7.3 ± 0.3	6.4 ± 0.3	4.8 ± 0.6	3.6 ± 1.0
Young's modulus, GPa	0.8 ± 0.1	1.1 ± 0.1	2.7 ± 0.2	1.1 ± 0.2
Flux, L m^{-2} h^{-1}	1403 ± 15	1934 ± 46	2522 ± 53	2646 ± 35
Permeability, L m^{-2} h^{-1} bar^{-1}	7019 ± 75	9672 ± 127	12613 ± 166	13234 ± 174

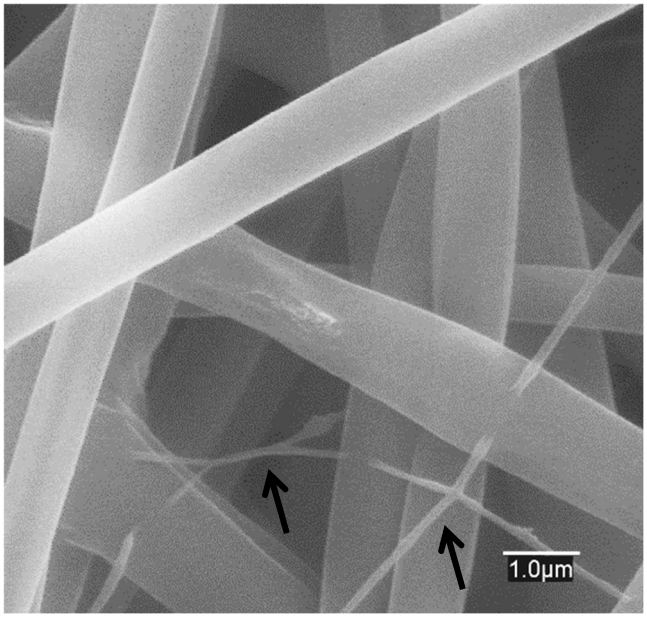

Figure S2. SEM micrographs of PAN/ChNC-15@PAN composite nanofibers (arrows pointing to secondary nanofibers).

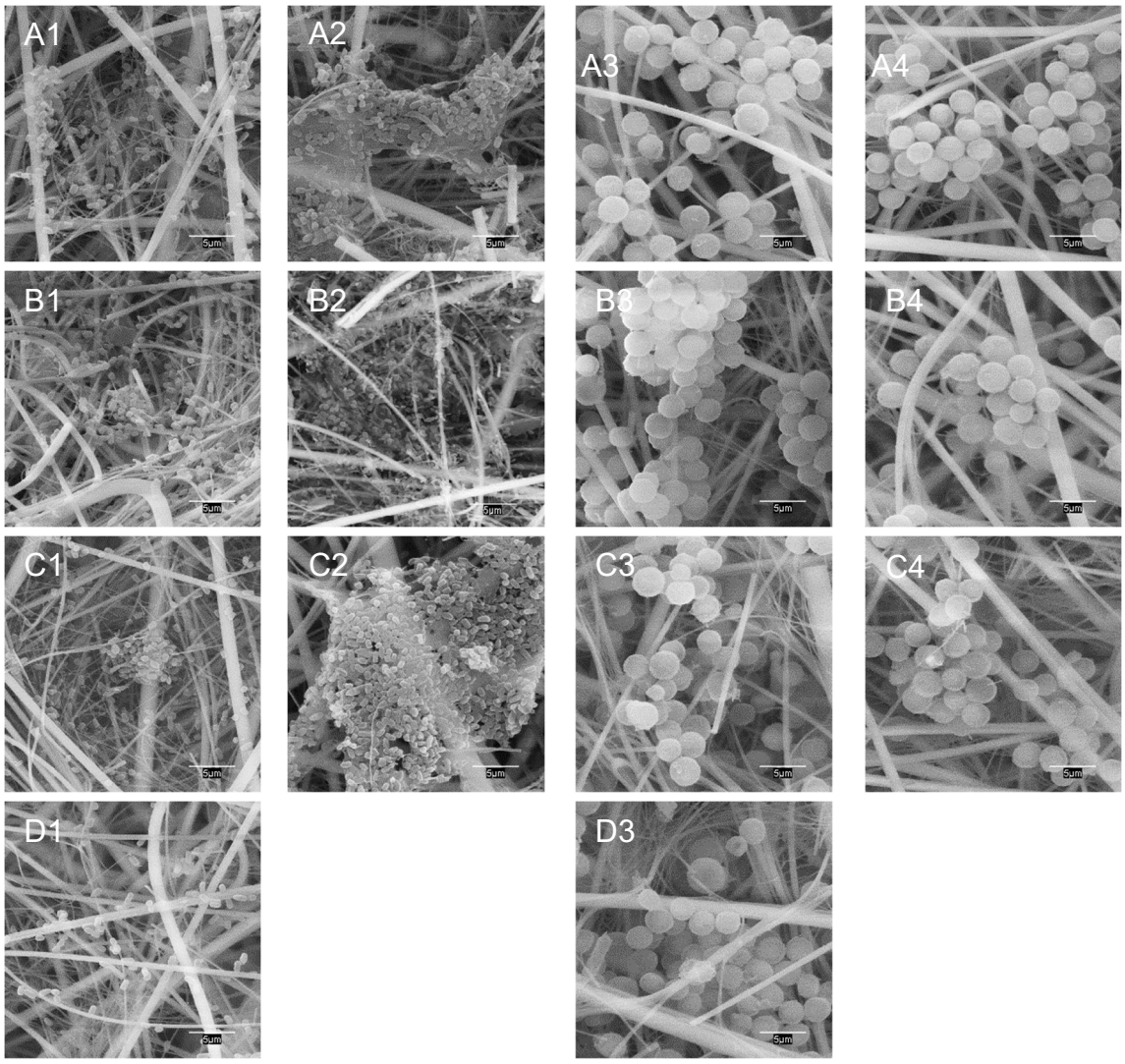

Figure S3. SEM images of PAN/CNC_{H2SO4}-15@PLA (A1, A3), PAN/CNC_{H2SO4}-20@PLA (A2, A4), PAN/CNC_{BE}-15@PLA (B1, B3), PAN/CNC_{BE}-20@PLA (B2, B4), PAN/ChNC-15@PLA (C1, C3), PAN/ChNC-20@PLA (C2, C4) and PLA (D1, D3) after filtration of *E. coli* cells (columns 1 and 2) and *A. niger* spores (columns 3 and 4).